Breaking the diffraction limit of light-sheet fluorescence microscopy by RESOLFT

Patrick Hoyer[a,b,c], Gustavo de Medeiros[c], Bálint Balázs[c,d], Nils Norlin[c], Christina Besir[c], Janina Hanne[a,b,e], Hans-Georg Kräusslich[e], Johann Engelhardt[a,b], Steffen J. Sahl[f], Stefan W. Hell[a,b,f,1], and Lars Hufnagel[c,1]

[a]Optical Nanoscopy Division, German Cancer Research Center, 69120 Heidelberg, Germany; [b]Bioquant, 69120 Heidelberg, Germany; [c]Cell Biology and Biophysics Unit, European Molecular Biology Laboratory, 69117 Heidelberg, Germany; [d]Faculty of Information Technology and Bionics, Pázmány Péter Catholic University, 1083 Budapest, Hungary; [e]Department of Infectious Diseases, Virology, University of Heidelberg, 69120 Heidelberg, Germany; and [f]Department of NanoBiophotonics, Max Planck Institute for Biophysical Chemistry, 37077 Göttingen, Germany

Edited by Xiaowei Zhuang, Harvard University/Howard Hughes Medical Institute, Cambridge, MA, and approved February 25, 2016 (received for review November 11, 2015)

We present a plane-scanning RESOLFT [reversible saturable/switchable optical (fluorescence) transitions] light-sheet (LS) nanoscope, which fundamentally overcomes the diffraction barrier in the axial direction via confinement of the fluorescent molecular state to a sheet of subdiffraction thickness around the focal plane. To this end, reversibly switchable fluorophores located right above and below the focal plane are transferred to a nonfluorescent state at each scanning step. LS-RESOLFT nanoscopy offers wide-field 3D imaging of living biological specimens with low light dose and axial resolution far beyond the diffraction barrier. We demonstrate optical sections that are thinner by 5–12-fold compared with their conventional diffraction-limited LS analogs.

light-sheet microscopy | RESOLFT | optical nanoscopy | 3D | live-cell imaging

Far-field nanoscopy (1, 2) methods discern features within subdiffraction distances by briefly forcing their molecules to two distinguishable states for the time period of detection. Typically, fluorophores are switched between a signaling "on" and a nonsignaling (i.e., dark) "off" state. Depending on the switching and fluorescence registration strategy used, these superresolution techniques can be categorized into coordinate-stochastic and coordinate-targeted approaches (2). The latter group of methods, comprising the so-called RESOLFT [reversible saturable/switchable optical (fluorescence) transitions] (1, 3–7) approaches, have been realized using patterns of switch-off light with one or more zero-intensity points or lines, to single out target point (zero-dimensional) or line (1D) coordinates in space where the fluorophores are allowed to assume the on state. The RESOLFT idea can also be implemented in the inverse mode, by using switch-on light and confining the off state. In any case, probing the presence of molecules in new sets of points or lines at every scanning step produces images.

Owing to the nature of the on and off states involved—first excited electronic and ground state—stimulated emission depletion (STED) (3) and saturated structured illumination microscopy (SSIM) (8), which both qualify as variants of the RESOLFT principle, typically apply light intensities in the range of MW/cm^2 and above. Especially when imaging sensitive samples where photoinduced changes must be avoided, RESOLFT is preferably realized with fluorophores which lead to the same factor of resolution improvement at much lower intensities of state-switching light. Reversibly switchable fluorescent proteins (RSFPs) are highly suitable for this purpose (4–7, 9), as transitions between their metastable on and off states require 5 orders of magnitude lower threshold intensities than STED/SSIM to guarantee switch-off. Suitable spectral properties, relatively fast millisecond switching kinetics, and high photostability of recently developed yellow-green-emitting RSFPs like rsEGFP (5), rsEGFP2 (7), and rsEGFP(N205S) (10) compared with early RSFPs have indeed enabled RESOLFT nanoscopy in living cells and tissues. To date, RSFP-based RESOLFT has achieved resolution improvements by factors of 4–5 in rsEGFP2-labeled samples (7). To further reduce the imaging time, massive parallelization of scanning has been reported (10). However, the diffraction-limited axial resolution and lack of background suppression restrict applications to thin samples.

Imaging applications typically require careful tuning of imaging parameters including speed, contrast, photosensitivity, and spatial resolution, depending on the information that is sought. Light-sheet fluorescence microscopy (LSFM) (11–15) stands out by its ability to balance most of these parameters for 3D imaging of living specimens. Recently reenacted as the selective plane illumination microscope (13), this microscopy mode has sparked increasing interest notably because of its short acquisition times in 3D imaging and low phototoxicity in living specimens. It excites fluorophores only in a thin diffraction-limited slice of the sample, perpendicular to the direction of fluorescence detection. The LS is generated by a cylindrical lens which focuses an expanded laser beam in only one direction onto the specimen or into the back-focal plane of an illumination objective. Alternatively, a single beam is quickly moved as a "virtual" LS (16) across a specimen section.

In such conventional LSFM imaging, the lateral resolution is determined by the numerical aperture (N.A.) of the detection objective (17), whereas axial resolution is given by the LS thickness, provided the latter is thinner than the axial extent of the point-spread function describing the imaging process from the focal plane of the detecting lens to the camera. In a previous study, the axial resolution of LSFM was pushed to the diffraction limit by using the full aperture of the illumination objective with Gaussian beams; this was carried out for practically useful combinations of

Significance

Light-sheet fluorescence microscopy (LSFM) is an imaging modality in which a sample is illuminated from the side by a beam engineered into a wide and relatively thin "sheet." This allows highly parallelized planewise scanning of volumes with inherent optical sectioning, offering a good balance between spatial and temporal resolution with reduced photostress. Unfortunately, the axial extent of the illuminated section is ultimately limited by diffraction. Here, we show that a RESOLFT [reversible saturable/switchable optical (fluorescence) transitions] strategy neutralizes the resolution-limiting role of diffraction in LSFM. While other LS strategies exist, which run into new hard axial limits of resolution, LS-RESOLFT is conceptually diffraction-unlimited and can be developed toward molecular-scale resolution.

Author contributions: P.H., S.J.S., S.W.H., and L.H. designed research; P.H. performed research; G.d.M., B.B., N.N., C.B., J.H., H.-G.K., and J.E. contributed new reagents/analytic tools; P.H. analyzed data; and P.H., S.J.S., and S.W.H. wrote the paper.

Conflict of interest statement: S.W.H. benefits through patents on the basic RESOLFT concept held by the Max Planck Society.

This article is a PNAS Direct Submission.

Freely available online through the PNAS open access option.

[1]To whom correspondence may be addressed. Email: shell@gwdg.de or hufnagel@embl.de.

This article contains supporting information online at www.pnas.org/lookup/suppl/doi:10.1073/pnas.1522292113/-/DCSupplemental.

N.A. (e.g., 0.8 for both illumination and detection objectives) permissible in light of the geometrical constraints given by the objective lens dimensions (18). High-N.A. illumination comes with short Rayleigh ranges of Gaussian beams, which inherently limit the field of view (FOV) along the direction of illumination. Scanned Bessel beams for diffraction-limited excitation with a virtual LS (19–21) typically offer larger FOVs (22), but side lobes broaden the scanned LS in the axial direction and contribute to phototoxicity outside of the focal plane of detection (20). A more complex approach has used Bessel-beam excitation in combination with structured illumination to obtain near-isotropic (but still diffraction-limited) resolution as measured on fluorescent beads (20), albeit at the cost of acquisition time and reduced contrast due to fluorescence generated by the side lobes. In different work, axial resolution has also been improved about fourfold by acquiring two complementary orthogonal views of the sample using two alternating LSs, followed by computationally fusing image information with a deconvolution incorporating both views (23). LS approaches have also helped suppress out-of-focus background for single-molecule imaging in biological situations (e.g., in ref. 24), including at superresolution (25–27).

Slight axial resolution improvement beyond the diffraction barrier has been demonstrated by overlapping a Gaussian excitation LS with a STED LS featuring a zero-intensity plane (28). Due to scattering and possibly additional aberrations caused by the wavelength difference between excitation and STED light, the maximal achievable resolution in biological specimens was severely limited. This was the case even in fixed samples. A successful application of LS-STED to living cells or organisms has not been reported. The relatively high average STED laser power required for high resolution gains calls for developing a coordinate-targeted superresolution LS approach with low-power operation, meaning a concept that does not solely rely on changing the way the light is directed to—or collected from—the sample, but a concept that harnesses an "on–off" transition for improved feature separation.

Results

Preparing the Fluorescent State by Reversible Fluorophore Switching in an LS Geometry. Here we report the simultaneous reversible switching between the fluorescent on and nonfluorescent off state in entire 2D planes, yielding LS-RESOLFT 3D images with much-improved axial (z) resolution. LS-RESOLFT symbiotically combines the advantages of RSFP-based RESOLFT nanoscopy and Gaussian-beam LS, exploiting the dark and fluorescent states of the RSFPs to reduce the axial extent of the examined object layer below the diffraction limit. This enables subdiffraction optical sectioning with low light intensities for detailed noninvasive imaging of living specimens. LS-RESOLFT also constitutes, to our knowledge, the first approach of improving the axial resolution in RSFP-based far-field fluorescence nanoscopy.

In the applied switching sequence (Fig. 1), so-called "negative-switching" RSFPs are switched to the on state with 405-nm light. Blue 488-nm light switches on-state fluorophores to the off state and also elicits fluorescence. The RSFPs applied in this study emit around 510 nm. The switching process is driven by three LSs in diffraction-limited axial sections of the sample. We use a common cylindrical lens, which focuses Gaussian laser beams into the back-focal plane of a low-N.A. illumination objective lens (Fig. S1). The activation LS switches RSFPs to the on state (Fig. 1 *A* and *B*). A second 488-nm LS featuring a planar zero-intensity domain leaves a subdiffraction thin section in which the fluorophores can assume the on state. The subdiffraction axial extent of the examined object layer is accomplished by switching fluorophores in the vicinity of this plane to the off state. Evidently, this plane is made to coincide with the focal plane of detection (Fig. 1 *C* and *D*). The off-switching pattern is generated by a half-moon phase plate (*SI Materials and Methods*) placed in the collimated off-switching beam. In the next step of the sequence, the remaining on-state fluorophores are read out by a third LS of the same wavelength (Fig. 1 *E* and *F*), which

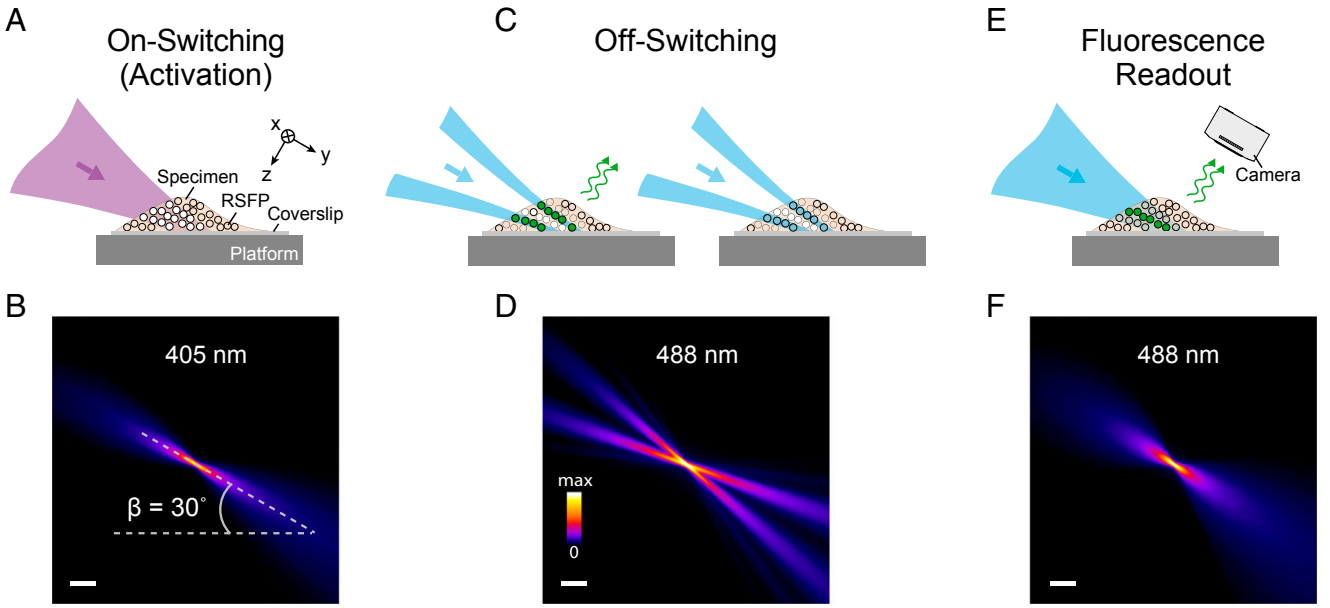

Fig. 1. LS-RESOLFT concept. A living specimen expressing RSFPs is grown on a coverslip mounted on a movable platform. The specimen is illuminated (here in y direction) perpendicular to the detection axis (z). (*A* and *B*) Only in a thin diffraction-limited section, RSFPs are switched from their initial off state (unfilled dots) to the on state (white dots) by an activating LS. None of the fluorophores outside the illuminated volume is affected by the laser light. (*C* and *D*) An LS featuring a central zero-intensity plane switches off the activated RSFPs above and below the detection focal plane (x-y). For negative-switching RSFPs, this is a competing process to fluorescence (green dots and arrows). For off-switching light intensities above the threshold of the RSFPs, only fluorophores within a slice of subdiffraction thickness remain activated. (*E* and *F*) These can be read out by a third LS and contribute to the LS-RESOLFT image. The platform is displaced to the next position in the scanning sequence for another illumination cycle (*A*, *C*, and *E*). (*B*, *D*, and *F*) Measured y-z cross-sections of the applied LSs visualized in fluorescent medium. The sheets impinge on the coverslip at an angle of 30°. (Scale bar, 100 μm.)

also switches them off again. Perpendicular to the illumination, a high-N.A. detection objective lens collects fluorescence in a wide-field manner. A tube lens focuses the detected light onto an sCMOS (scientific complementary metal-oxide-semiconductor) camera chip (lateral sampling of 108.3 nm). Images are recorded by displacing (scanning) the platform with the mounted coverslip and the sample at a design angle of 30° with respect to the illumination axis through the stationary LSs. The above acquisition cycle is repeated for each section of the sample, with the step size of the piezoelectric stage defining the axial sampling of the specimen (Fig. S2). The Rayleigh range along the illumination axis and the width of the LSs (Fig. S3) determine the FOV per plane; the maximal scan range of the piezoelectric stage defines the detectable volume.

Axial Resolution of LS-RESOLFT. We characterized the resolving power of the LS-RESOLFT nanoscope by imaging spherical HIV-1 particles carrying roughly 1,000 rsEGFP2 proteins embedded in the HIV-1 structural protein Gag (group-specific antigen) (29) (Fig. 2 *A* and *B* and Movie S1). For a sufficiently high off-switching intensity, the axial resolution of the LS-RESOLFT instrument is increased to values well below the diffraction limit. The FWHM of a Gaussian fit to the axial line profile through a single HIV-1 particle is reduced from 1,522 nm for diffraction-limited LSFM to 124 nm in LS-RESOLFT (Fig. S4), demonstrating an increase in axial resolution by a factor >12. If the average HIV-1 particle size of 120–130 nm is taken into account, a RESOLFT LS thickness of about 100 nm (FWHM) is obtained. In a dense sample, single HIV-1 particles are clearly separable in the LS-RESOLFT image at subdiffraction distances, whereas they are not separable in the conventional LSFM mode. The theoretically predicted square-root dependence (1) of axial resolution on the off-switching power was experimentally confirmed (Fig. 2*C*). FWHM values obtained by averaging over more than 200 sparsely distributed particle images across the entire lateral FOV depend on the square root of the off-switching power (Fig. S5).

We conclude that the axial resolution is not limited conceptually, but merely by the available off-switching power and, more crucially, the photophysical properties of the present RSFPs. Designed for axial resolution improvement, the results presented in Fig. 2*C* additionally suggest a moderate (up to ~15%) decrease in extracted particle diameters along the lateral direction by LS-RESOLFT (at maximal switch-off power). We maintain that this is due to better definition of the objects owing to improved image contrast. Importantly, FWHM values measured at different positions along the illumination axis indicate that the Rayleigh range of the RESOLFT LS is sufficiently long to uniformly switch-off fluorophores in an entire section of a cell (Fig. 2*D*).

We also demonstrate the imaging capabilities of LS-RESOLFT on the cytoskeleton of living HeLa cells (Fig. 3 *A*–*C*, Fig. S7, and Movies S2 and S3). The structural protein keratin-19 was labeled by fusion of the recently developed rsEGFP variant rsEGFP(N205S), which has slower off-switching kinetics than other rsEGFPs but, at

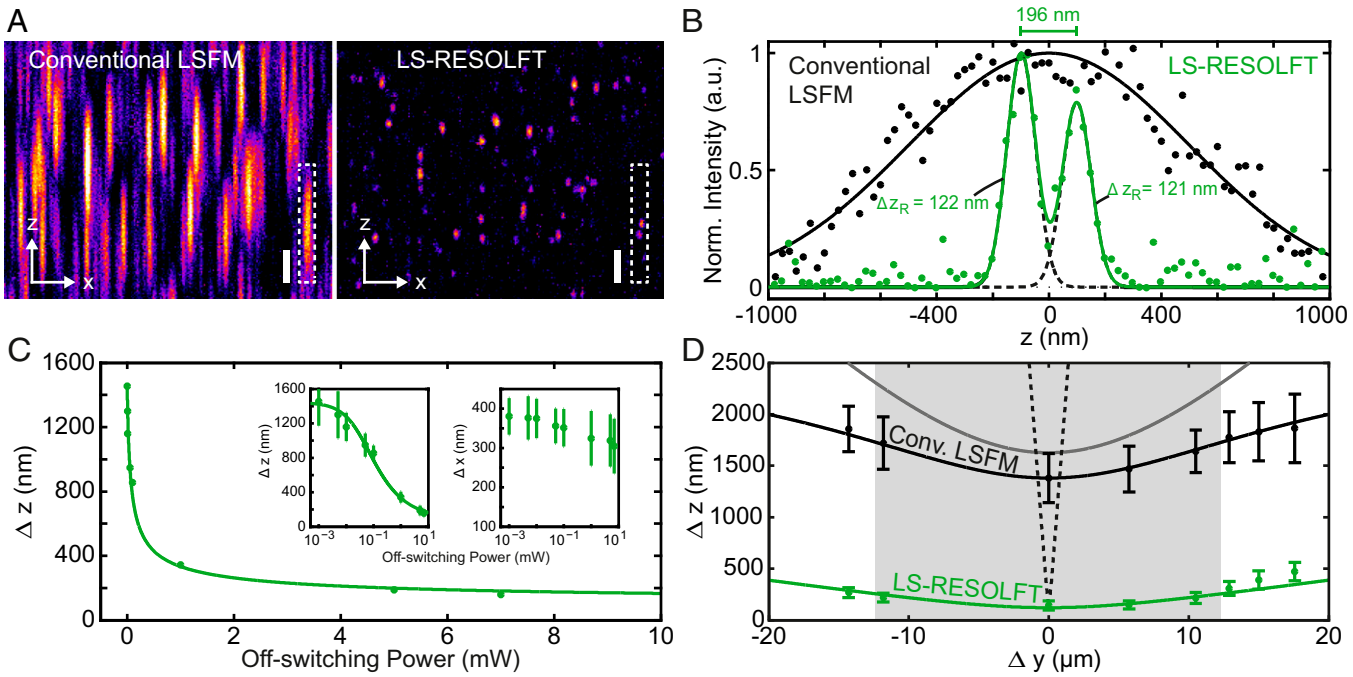

Fig. 2. Characterization of LS-RESOLFT with spherical HIV-1 particles, in comparison with the conventional LSFM mode. (*A*) An *x*-*z* cross-section through a typical 3D image stack of HIV-1 particles attached to a glass coverslip clearly shows the improvement in *z* resolution enabled by LS-RESOLFT. Note that pixels correspond to 108.3 nm in *x* and 25 nm in *z*, respectively (total image size: $24 \times 4\ \mu m^2$). (Scale bar width and height, 500 nm.) (*B*) Pixel intensity line profile along the *z* direction in a marked region in *A* (white dashed box) for LS-RESOLFT (green dots) in comparison with conventional LSFM (black dots), with single (black line) and double (green line) Gaussian fits to the data. The FWHMs of single Gaussian fits (dashed black line) to the LS-RESOLFT data are far below the (axial) diffraction limit. (*C*) Dependence of the resolving power Δz on the off-switching laser power. For a fixed off-switching time of 30 ms, the average axial FWHMs of HIV-1 particles imaged in LS-RESOLFT mode were determined for various powers of the switch-off light bounding the axial zero-intensity plane. Mean FWHM values are plotted versus off-switching power in the back-focal plane of the illumination objective (green dots). Fit (green line) to the data confirms the inverse scaling with the square root of the applied intensity. The same data and fit are shown on a logarithmic scale (*Left Inset*), together with error bars derived from the SD of a Gaussian fit to the histograms (Fig. S5). (*Right Inset*) Lateral (*x*-*y*) FWHM dependence on off-switching power is shown (see the text). (*D*) At several positions along the illumination axis of the LSs, the average axial FWHM of the HIV-1 images were determined. The distance Δy in the measured sample plane from the minimal beam waist position is derived by the method shown in Fig. S6. The average value of Δz together with the SD is plotted versus the measured value of Δy for conventional LSFM (black data points) and LS-RESOLFT (green data points). From a fit to the conventional LSFM data (black line), the experimentally realized (diffraction-limited) illumination profile is inferred (gray line) for an illuminating Gaussian LS and a (near-) Gaussian axial detection profile. The FOV (gray box) of the microscope is then defined by the increase in waist by $\sqrt{2}$ -fold to both sides. For reference, the FWHM beam waist of a theoretical Gaussian LS with the same minimum value as achieved by RESOLFT is plotted versus Δy (black dashed line). LS-RESOLFT substantially extends the available FOV along the *y* direction.

the same time, offers more photons per unit time when in the on state. After activation at 350 μW for 10 ms, the double-sheeted off-switching beam (6.9 mW) was applied for 100 ms, followed by readout for 60 ms at 150 μW. All powers were measured close to the back-focal plane of the illumination objective. To directly visualize the improvement in resolution, a conventional LSFM image is subsequently taken at the same scan position (activated and read out with the same light doses and exposure times as for the LS-RESOLFT image, yet without off-switching). LS-RESOLFT imaging of NUP214, a constituent protein of the nuclear pore complex fused to three rsEGFP(N205S) proteins in living U2OS cells, shows a gain in resolution by a factor of 5.6 (Fig. 3 *D*–*F*). The advantage of reduced photobleaching that is typical of standard LSFM and benefits long-term acquisition of samples is conserved in LS-RESOLFT (Fig. S8). Phototoxic effects induced by the RESOLFT imaging protocol were certainly minimal, as imaged cells kept dividing after imaging (Fig. S9).

Discussion and Conclusions

We have demonstrated RESOLFT LS nanoscopy, enabling inherently parallelized 3D imaging with subdiffraction axial resolution. Several living samples labeled with one of the recently developed rsEGFP variants were recorded at low light intensity levels. The axial resolution of LS-RESOLFT is superior to any other LSFM variants, such as Bessel-beam LSs or implementations based on structured illumination, which do not implement molecular-state transitions for feature separation—and therefore do not neutralize the resolution-limiting role of diffraction (19–21, 30). A sample- and power-dependent improvement by a factor of 5–12 has already been achieved, which clearly

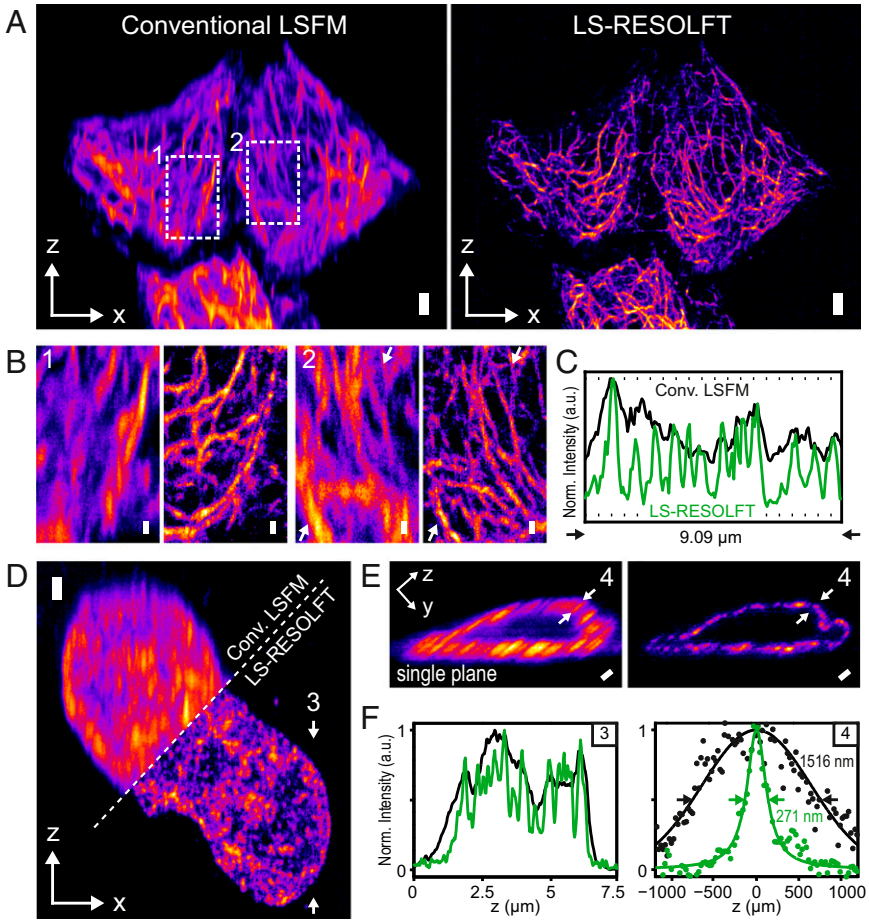

Fig. 3. Conventional LSFM and LS-RESOLFT images of the keratin-19 network and a structural protein of the nuclear pore complex in living cells. (*A*–*C*) The superior resolving power of LS-RESOLFT is demonstrated in *x*-*z* maximum intensity projections of a recorded image stack showing keratin-19 filaments tagged with rsEGFP(N205S) in HeLa cells. A stack of 1,200 images per imaging technique was recorded with a step size of 50 nm, which results in a total volume of $82 \times 47 \times 30\ \mu m^3$. The voxel size is set to $108.3 \times 108.3 \times 50\ nm^3$ [($\Delta x = 108.3 \times \Delta z = 50$) nm are represented as square pixels; versions with isotropic pixels in Fig. S10]. (*A*) The LS-RESOLFT image exhibits much thinner features than conventional LSFM; keratin-19 strands are clearly separable even in dense areas. (Scale bar width and height, 2 μm.) (*B*) Zoom-ins on two areas in the sample highlight the imaging capabilities of LS-RESOLFT. They show an *x*-*z* area of $10.7 \times 7.8\ \mu m^2$. (Scale bar width and height, 500 nm.) (*C*) Normalized intensity profiles along the line between the white arrowheads in zoom-in 2 reveal individual peaks for separated keratin-19 strands in the LS-RESOLFT mode (green) which cannot be resolved in conventional LSFM (black). (*D*) Maximum intensity projections along the illumination axis *y* of a living U2OS cell expressing Nup214-3x-rsEGFP(N205S) are shown for conventional LSFM and LS-RESOLFT. A stack of 400 images was recorded with a step size of 50 nm, which results in a total volume of $43 \times 34 \times 20\ \mu m^3$. The voxel size is set to $108.3 \times 108.3 \times 50\ nm^3$. Square pixels with the above sampling are displayed. (Scale bar width and height, 1 μm.) (*E*) The resolution enhancement by RESOLFT (*Right*) compared with conventional LSFM (*Left*) is highlighted in a single *y*-*z* section through the nucleus. Note that for display the image was rotated by 30° around the *x* axis. (Scale bar width and height, 1 μm.) (*F*) A line profile along the direction indicated by the arrowheads in *D* is plotted. Enabled by a RESOLFT LS thickness below the diffraction limit, LS-RESOLFT (green line) reveals distinct peaks which cannot be distinguished in diffraction-limited conventional LSFM (black line). A line profile through a nuclear pore complex marked in *E* is plotted for the diffraction-limited LSFM (black dots) and LS-RESOLFT (green dots) modes. Gaussian (black) and Lorentzian (green) fits to the conventional LSFM and LS-RESOLFT data points, respectively, reveal an increase in axial resolution of more than a factor of 5 for LS-RESOLFT.

outperforms the previous STED-LS approach, where a gain in axial resolution by <1.5-fold was reported for dye-filled particles only, and at much higher light doses (28).

Clearly, the spatial resolution (i.e., information) increase—as it necessitates a greater number of sampling steps in space to satisfy Nyquist, and as it requires time to perform the state switching—must be inevitably accompanied by an overall somewhat reduced acquisition rate. This is a common inherent feature of all nanoscopy approaches separating neighboring fluorophores by on–off transitions (2). As in all RESOLFT approaches, however, spatial resolution is—advantageously—readily and freely tunable (compare Fig. 2*C*), and fewer steps may be sampled in space at accordingly faster rates per volume stack. At ∼100 ms per frame, recording speed in this first demonstration is up to about an order of magnitude slower than conventional LS imaging, which reads out coarser fluorescent volumes. Note that the physical reduction by LS-RESOLFT of the specimen section in which the fluorescent on state remains allowed per scanning step implies on average fewer fluorophores present per section. Examination of typical images with LS-RESOLFT revealed signal-to-background ratios between ∼3:1 and ∼12:1 for imaging experiments with HIV-1 particles depending on label incorporation, and ∼7:1 to ∼12:1 for keratin strands (comparing to directly neighboring dark regions)—at the conservatively chosen frame durations in these proof-of-principle experiments. Ongoing improvements in switchable fluorophore characteristics, notably in terms of fluorescence quantum yield and switching speed, are expected to further improve temporal resolution of the RESOLFT approaches in general, including this highly parallelized LS variant.

The capability to create optical sections of ∼100-nm thickness is similar to the axial resolving power of a typical TIRF (total internal reflection fluorescence) microscope, yet with a decisive difference: Whereas TIRF produces only one slice that is tightly confined to the coverslip surface, LS-RESOLFT offers subdiffraction axial resolution in any slice throughout the entire specimen and can thus be applied to a broad range of (not just) cell-biological questions. Due to the low off-switching intensities, LS-RESOLFT allows live-cell imaging of biological samples over extended time periods. Large FOVs are possible, as entire planes are being captured at once, without the need for sequential lateral readout. Acquisition time is thus reduced by a factor given by the number of pixels per FOV compared with confocal "*z*-doughnut" RESOLFT strategies achieving similar *xyz* resolution for identical volumes (*SI Materials and Methods*). Because off-switching and readout are performed at the same wavelength, potential chromatic aberrations are inherently avoided. Recordings with spectrally distinct RSFPs will in the future allow colocalization studies in subdiffraction volumes. Looking ahead, LS-RESOLFT can be equipped with an option to additionally superresolve along the lateral dimensions. Because the present LS-RESOLFT design employs independent beam paths for illumination and detection of the sample, the same concepts which lead to conceptually diffraction-unlimited lateral resolution and use wide-field detection can also be applied to LS-RESOLFT. One possible approach combines LS-RESOLFT with the previously demonstrated parallelized 2D RESOLFT technique (10).

Materials and Methods

Detailed descriptions of the optical setup, the image acquisition and representation, sample preparation including mammalian cell culture, as well as a discussion of the acquisition speed gains enabled by the highly parallelized LS readout, are provided in *SI Materials and Methods*. In brief, LS-RESOLFT nanoscopy at low light levels was demonstrated with custom-built optics, featuring two water-dipping objective lenses in perpendicular configuration: an illumination objective (10×/0.3 N.A.) to create three LSs for activation, off-switching, and readout of RSFPs, and a detection objective (40×/0.8 N.A.) for collection of sample fluorescence in the wide field. Laser beam paths were coaligned, expanded, and focused by a common cylindrical lens into the back aperture of the illumination objective. The activation (405 nm) and readout (488 nm) LSs featured conventional geometries. The switch-off beam (488 nm) was modulated by a phase retardation plate (Fig. S1) to produce, after focusing by the objective, an off-switching light distribution with a central plane of minimal intensity (the "zero"). Scanning of the specimen through the LSs acquired images plane by plane.

ACKNOWLEDGMENTS. We thank Jan Ellenberg and Anna Szymborska-Mell (both European Molecular Biology Laboratory) for vectors, and Barbara Müller (Heidelberg University) for vectors and cloning, and all of them, as well as Tim Grotjohann (Max Planck Institute for Biophysical Chemistry), for helpful discussions. S.W.H. acknowledges the Federal Ministry of Education and Research for funding this work within the project STEDlight (FKZ:13N11173).

1. Hell SW (2003) Toward fluorescence nanoscopy. *Nat Biotechnol* 21(11):1347–1355.
2. Hell SW (2009) Microscopy and its focal switch. *Nat Methods* 6(1):24–32.
3. Hell SW, Wichmann J (1994) Breaking the diffraction resolution limit by stimulated emission: Stimulated-emission-depletion fluorescence microscopy. *Opt Lett* 19(11):780–782.
4. Hofmann M, Eggeling C, Jakobs S, Hell SW (2005) Breaking the diffraction barrier in fluorescence microscopy at low light intensities by using reversibly photoswitchable proteins. *Proc Natl Acad Sci USA* 102(49):17565–17569.
5. Grotjohann T, et al. (2011) Diffraction-unlimited all-optical imaging and writing with a photochromic GFP. *Nature* 478(7368):204–208.
6. Brakemann T, et al. (2011) A reversibly photoswitchable GFP-like protein with fluorescence excitation decoupled from switching. *Nat Biotechnol* 29(10):942–947.
7. Grotjohann T, et al. (2012) rsEGFP2 enables fast RESOLFT nanoscopy of living cells. *eLife* 1:e00248.
8. Gustafsson MGL (2005) Nonlinear structured-illumination microscopy: Wide-field fluorescence imaging with theoretically unlimited resolution. *Proc Natl Acad Sci USA* 102(37):13081–13086.
9. Schwentker MA, et al. (2007) Wide-field subdiffraction RESOLFT microscopy using fluorescent protein photoswitching. *Microsc Res Tech* 70(3):269–280.
10. Chmyrov A, et al. (2013) Nanoscopy with more than 100,000 'doughnuts'. *Nat Methods* 10(8):737–740.
11. Voie AH, Burns DH, Spelman FA (1993) Orthogonal-plane fluorescence optical sectioning: Three-dimensional imaging of macroscopic biological specimens. *J Microsc* 170(Pt 3):229–236.
12. Fuchs E, Jaffe J, Long R, Azam F (2002) Thin laser light sheet microscope for microbial oceanography. *Opt Express* 10(2):145–154.
13. Huisken J, Swoger J, Del Bene F, Wittbrodt J, Stelzer EHK (2004) Optical sectioning deep inside live embryos by selective plane illumination microscopy. *Science* 305(5686):1007–1009.
14. Dodt H-U, et al. (2007) Ultramicroscopy: Three-dimensional visualization of neuronal networks in the whole mouse brain. *Nat Methods* 4(4):331–336.
15. Wu Y, et al. (2011) Inverted selective plane illumination microscopy (iSPIM) enables coupled cell identity lineaging and neurodevelopmental imaging in Caenorhabditis elegans. *Proc Natl Acad Sci USA* 108(43):17708–17713.
16. Keller PJ, Stelzer EHK (2008) Quantitative in vivo imaging of entire embryos with digital scanned laser light sheet fluorescence microscopy. *Curr Opin Neurobiol* 18(6):624–632.
17. Engelbrecht CJ, Stelzer EH (2006) Resolution enhancement in a light-sheet-based microscope (SPIM). *Opt Lett* 31(10):1477–1479.
18. Capoulade J, Wachsmuth M, Hufnagel L, Knop M (2011) Quantitative fluorescence imaging of protein diffusion and interaction in living cells. *Nat Biotechnol* 29(9):835–839.
19. Fahrbach FO, Simon P, Rohrbach A (2010) Microscopy with self-reconstructing beams. *Nat Photonics* 4(11):780–785.
20. Planchon TA, et al. (2011) Rapid three-dimensional isotropic imaging of living cells using Bessel beam plane illumination. *Nat Methods* 8(5):417–423.
21. Gao L, et al. (2012) Noninvasive imaging beyond the diffraction limit of 3D dynamics in thickly fluorescent specimens. *Cell* 151(6):1370–1385.
22. Durnin J, Miceli JJ, Jr, Eberly JH (1988) Comparison of Bessel and Gaussian beams. *Opt Lett* 13(2):79–80.
23. Wu Y, et al. (2013) Spatially isotropic four-dimensional imaging with dual-view plane illumination microscopy. *Nat Biotechnol* 31(11):1032–1038.
24. Siebrasse JP, Kaminski T, Kubitscheck U (2012) Nuclear export of single native mRNA molecules observed by light sheet fluorescence microscopy. *Proc Natl Acad Sci USA* 109(24):9426–9431.
25. Zanacchi FC, et al. (2011) Live-cell 3D super-resolution imaging in thick biological samples. *Nat Methods* 8(12):1047–1049.
26. Zhao ZW, et al. (2014) Spatial organization of RNA polymerase II inside a mammalian cell nucleus revealed by reflected light-sheet superresolution microscopy. *Proc Natl Acad Sci USA* 111(2):681–686.
27. Galland R, et al. (2015) 3D high- and super-resolution imaging using single-objective SPIM. *Nat Methods* 12(7):641–644.
28. Friedrich M, Gan Q, Ermolayev V, Harms GS (2011) STED-SPIM: Stimulated emission depletion improves sheet illumination microscopy resolution. *Biophys J* 100(8):L43–L45.
29. Carlson LA, et al. (2008) Three-dimensional analysis of budding sites and released virus suggests a revised model for HIV-1 morphogenesis. *Cell Host Microbe* 4(6):592–599.
30. Chen BC, et al. (2014) Lattice light-sheet microscopy: Imaging molecules to embryos at high spatiotemporal resolution. *Science* 346(6208):1257998.
31. Lampe M, et al. (2007) Double-labelled HIV-1 particles for study of virus-cell interaction. *Virology* 360(1):92–104.
32. Müller B, et al. (2004) Construction and characterization of a fluorescently labeled infectious human immunodeficiency virus type 1 derivative. *J Virol* 78(19):10803–10813.